



The Abdus Salam
International Centre for Theoretical Physics


United Nations
Educational, Scientific
and Cultural Organization


International Atomic
Energy Agency



SMR.1676 - 4

8th Workshop on Non-Linear Dynamics and Earthquake Prediction

3 - 15 October, 2005

Modeling of Block-and-Fault System Dynamics and Seismicity: Description of the Model and Application to the Tibut-Himalayan Region

Alexandre A. Soloviev
Russian Academy of Sciences
International Inst. of Earthquake Prediction Theory and
Matemtical Geophysics
Warshavskoye Sh. 79. Kor2
117556 Moscow
Russia

These are preliminary lecture notes, intended only for distribution to participants

Modeling of Block-and-Fault System Dynamics and Seismicity: Description of the Model and Application to the Tibet-Himalayan Region

A. Ismail-Zadeh (1, 2), J.-L. Le Mouél (1), A. Soloviev (2), P. Tapponnier (1), and I. Vorovieva (2)

**(1) Institut de Physique du Globe de Paris
4 Place Jussieu, 75252 Paris, France
www.ipgp.jussieu.fr**

**(2) International Institute of Earthquake Prediction
Theory and Mathematical Geophysics
Russian Academy of Sciences
Warshavskoye sh. 79, kor. 2, Moscow 117556
Russian Federation
www.mitp.ru**

ABSTRACT

A model of block-and-fault system dynamics (or simpler "block model") considers a seismic region as a system of perfectly rigid blocks divided by infinitely thin plane faults. The blocks interact between themselves and with the underlying medium. The system of blocks moves as a consequence of prescribed motion of the boundary blocks and of the underlying medium. As the blocks are perfectly rigid, all deformation takes place in the fault zones and at the block base in contact with the underlying medium. Relative block displacements take place along the fault planes. This assumption is justified by the fact that for the lithosphere the effective elastic moduli of the fault zones are significantly smaller than those within the blocks. Block motion is defined so that the system is in a quasistatic equilibrium state. The interaction of blocks along the fault planes is viscous-elastic ("normal state") while the ratio of the stress to the pressure remains below a certain strength level. When the critical level is exceeded in some part of a fault plane, a stress-drop ("failure") occurs (in accordance with the dry friction model), possibly causing failure in other parts of the fault planes. These failures produce earthquakes. Immediately after the earthquake and for some time after, the affected parts of the fault planes are in a state of creep. This state differs from the normal state because of a faster growth of inelastic displacements, lasting until the stress falls below some other level. This modeling gives rise a synthetic earthquake catalogue.

The Tibetan plateau and Himalayans have resulted from the continuous Indian and Eurasian plate convergence following their initial collision at about 55 million years ago. Earthquakes in the region occur mainly in response to the crustal motion and stress localization associated with this convergence. To understand the basic features of the motion and seismicity in the Tibet-Himalayan region, we develop the block model that is composed of twelve interacting upper crustal blocks. These blocks move as a consequence of the Indian plate push. We develop several sets of numerical experiments constrained by the regional seismic observations, geodetic and geological data. Synthetic large events in the numerical experiments are clustered mainly on the fault segments associated with the Himalayan Frontal Thrust as well as at some internal faults of the Tibetan plateau. The clustering of earthquakes at some fault is a consequence of dynamics of the regional fault system rather than that of the fault only. We show that variations in the relationship of magnitude to frequency of the events depend on changes in the motion of the upper crustal blocks and on the rheological properties of the lower crust and fault zones. We demonstrate in the model that the present crustal motion in the region is characterized by the north-northeastern movement of India toward Eurasia. Fluctuations in rheological properties of fault plane zones and/or the lower crust influence displacement rates of the crustal blocks and hence slip rates at the faults separating the blocks. This can explain the discrepancies in estimates of slip rates at major faults in the region (e.g., Altyn Tagh, Karakorum) over short and long time scales.

I. INTRODUCTION

A model of block-and-fault system dynamics (or simpler “block model”) of the lithosphere was developed to analyse features of seismicity in a particular region. A structure, which consists of perfectly rigid blocks connected by thin viscous-elastic layers (“faults”), is considered in the model. The blocks interact between themselves and with the underlying medium. The system of blocks moves as a consequence of prescribed motion of the boundary blocks and of the underlying medium. The detailed description of the model is given below.

The model exploits the hierarchical block structure of the lithosphere proposed by *Alekseevskaya et al.* (1977). The basic principles of the model were developed by *Gabrielov et al.* (1986, 1990) on the basis of the proposition that blocks of the lithosphere are separated by comparatively thin, weak and less consolidated fault zones, such as lineaments and tectonic faults, and major deformation and most earthquakes occur in such fault zones. The model takes advantage of the simple fact that the integral rigidity of the fault zones is smaller than the blocks (at least in the time scale smaller than say 100 years or less). Accordingly, blocks are presumed absolutely rigid.

Later on the model was improved to create possibility of approximating in it a block structure of a real seismoactive region under consideration (*Soloviev 1995*), and now it is region-specific and allows to set up specific driving tectonic forces, the realistic geometry of blocks and fault network, and the rheology of fault zones. The model generates stick-slip movement of blocks, comprising seismicity and slow movements.

The model reproduces the whole ensemble: tectonic driving forces => geodetic movements => creep => earthquakes.

The block model as other numerical models of the processes generating seismicity (e.g., *Shaw et al. 1992; Gabrielov and Newman 1994; Allègre et al. 1995; Newman et al. 1995; Turcotte 1997; Narteau et al. 2000*) provides a straightforward tool for a broad range of problems: (i) connection of seismicity and geodynamics; (ii) dependence of seismicity on general properties of fault networks; that is, fragmentation of structure, rotation of blocks, direction of driving forces etc; (iii) study of the earthquake preparation process and earthquake prediction (e.g., *Gabrielov and Newman 1994*), moreover such models can be used to suggest new premonitory patterns that might exist in real catalogs (e.g., *Gabrielov et al. 2000; Shebalin et al. 2000*).

The block model reproduces some basic features of the observed seismicity: Gutenberg-Richter law, clustering of earthquakes, dependence of the occurrence of large earthquakes on fragmentation of the block structure and on rotation of blocks etc. It enables to study relations between geometry of faults, block movements and earthquake flow, and to reproduce regional features of seismicity. From simplest observation - territorial distribution of seismicity - the model enables to reconstruct tectonic driving forces (and to evaluate competing geodynamic hypotheses).

In the absence of seismicity the block model enables to study dependence between motions of boundary blocks specified at lateral boundaries of the structure, motions of the underlying medium specified at the block bottoms and motions of the blocks constituting the structure. One may consider the direct problem: to determine motions of the blocks constituting the structure (and their relative motions along the faults) when motions of the underlying medium and the boundaries are specified. The inverse problem may be considered as well: to determine motions of the underlying medium and the boundaries, which supply the best approximation of the specified motions of the blocks of the structure or their relative motions along the faults.

The detailed description of the block model and examples of its application are given by *Soloviev and Ismail-Zadeh (2003)*. The model was used to analyze clustering of

earthquakes (*Maksimov and Soloviev, 1999*), a dependence of the occurrence of large earthquakes on a fragmentation of the structure and on rotation of blocks (*Keilis-Borok et al., 1997*), the lithospheric motion and seismic flow in the Vrancea earthquake-prone region of the southeastern Carpathians (*Panza et al., 1997; Soloviev et al., 1999; Ismail-Zadeh et al., 1999*), in the Western Alps, and in Sunda Arc (*Soloviev and Ismail-Zadeh, 2003*).

Following the closure of the Mesozoic Tethys ocean, the India–Asia collision initiated the development of the Himalayan range and the Tibetan plateau and induced widespread strain in southeastern Asia and China. The Tibetan plateau is underlain by a thick crust (up to 70 to 80 km) as inferred from gravity anomalies and seismic profiles (*Barazangi and Ni, 1982; Hirn et al., 1984; Le Pichon et al., 1992; Nelson et al., 1996*). The Himalayan front and the Longmen Shan represent abrupt and steep topographic fronts at the southern and eastern edges of the plateau (Fig. 1). Remarkable features of the Tibetan plateau are its flat topography and predominantly strike-slip faulting (e.g., Altyn-Tagh, Karakorum, Kunlun, Xianshuihe, Red River faults) (*Molnar and Tapponnier, 1978; Tapponnier et al., 1981; Armijo et al., 1986, 1989; Peltzer and Tapponnier, 1988; Avouac and Tapponnier, 1993; Fielding et al., 1994; England and Molnar, 1997a,b*).

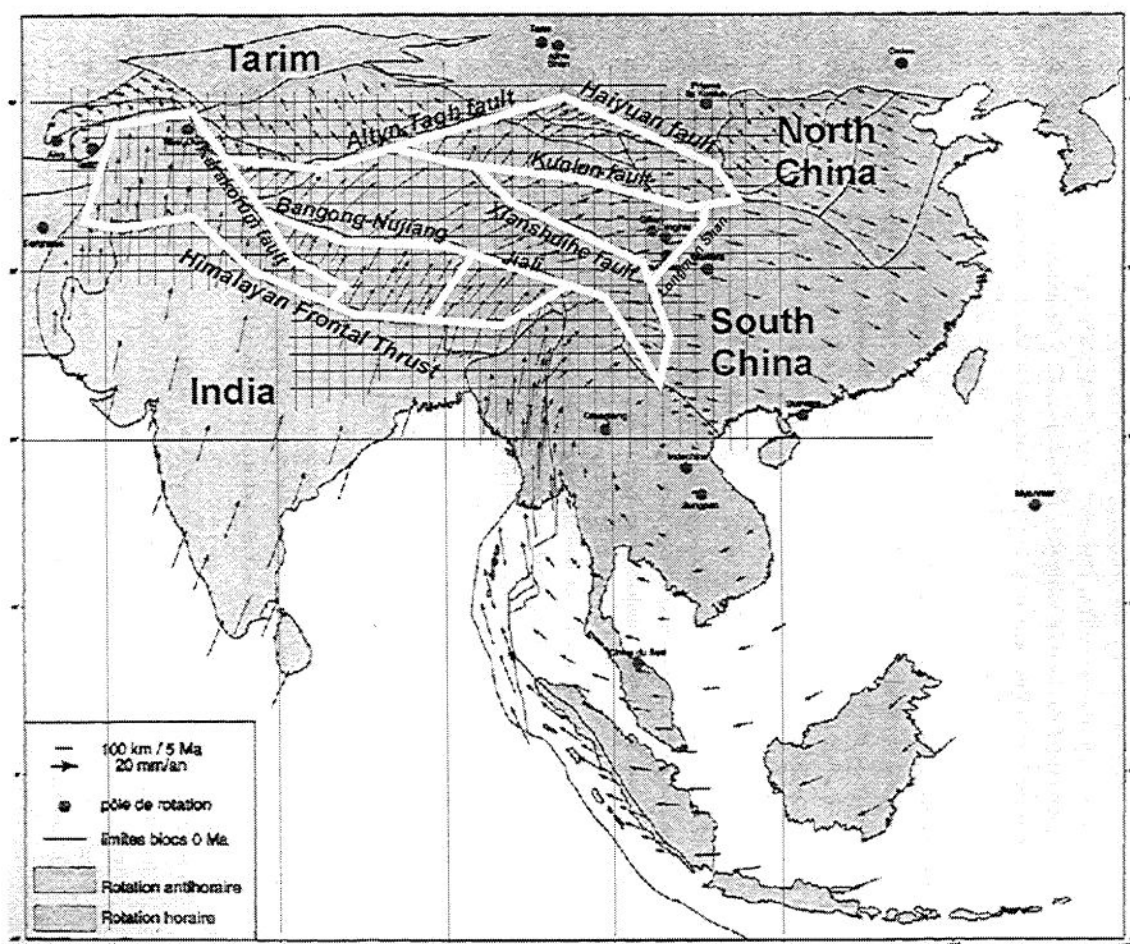


FIGURE 1 Observed movements and principal faults of Tibet and adjacent regions. Thick lines present the model structure.

There are three distinct views of the active deformation in the region that dominate the debate on the mechanics of continental deformation. One view is that the deformation is

distributed throughout the continental lithosphere (e.g., *Houseman and England, 1996; England and Molnar, 1997a,b*). Another view is associated with the crustal thinning and the deformation dominated by a flow in a channel within the mid-to-lower crust (*Bird, 1991; Royden et al., 1997; Clark and Royden, 2000; Beaumont et al., 2001*). Meanwhile there is mounting evidence supporting an alternative view that a substantial part of the deformation of the continents is localized on long and relatively narrow faults and shear zones separating rigid crustal blocks (e.g., *Tapponnier et al., 1982, 2001; Peltzer and Saucier, 1996; McClusky et al., 2000*). Many of these zones cut the base of the crust (*Vergnes et al., 2002; Wittlinger et al., 2004*), and some extend to the base of the lithosphere (e.g., *Wittlinger et al., 1998*). Therefore such deformation can be described by motions of crustal blocks separated by those faults that gives possibility to use the block model to study seismic patterns and fault slip rates in the Tibet-Himalayan region.

In the study we have tried to answer the following questions: (i) how upper crustal blocks of the Tibetan plateau react on the Indian plate motion; (ii) how earthquakes cluster at the regional fault system; and (iii) how rheological properties of the lower crust and fault zones influence the earthquake flow and fault slip rates.

II. MODEL OF BLOCK-AND-FAULT SYSTEM DYNAMICS

The definitions used in the block model and its formal mathematical description are given below.

2.1 Block Structure Geometry

A layer with thickness H limited by two horizontal planes is considered (Fig. 2), and a block structure is defined as a limited and simply connected part of this layer. Each lateral boundary of the block structure is defined by portions of the parts of planes intersecting the layer. The subdivision of the structure into blocks is performed by planes intersecting the layer. The parts of these planes, which are inside the block structure and its lateral faces, are called "fault planes".

The geometry of the block structure is defined by the lines of intersection between the fault planes and the upper plane limiting the layer (these lines are called "faults"), and by the angles of dip of each fault plane. Three or more faults cannot have a common point on the upper plane, and a common point of two faults is called "vertex". The direction is specified for each fault and the angle of dip of the fault plane is measured on the left of the fault. The positions of a vertex on the upper and the lower plane, limiting the layer, are connected by a segment ("rib") of the line of intersection of the corresponding fault planes. The part of a fault plane between two ribs corresponding to successive vertices on the fault is called "segment". The shape of the segment is a trapezium. The common parts of the block with the upper and lower planes are polygons, and the common part of the block with the lower plane is called "bottom".

It is assumed that the block structure is bordered by a confining medium, whose motion is prescribed on its continuous parts comprised between two ribs of the block structure boundary. These parts of the confining medium are called "boundary blocks".

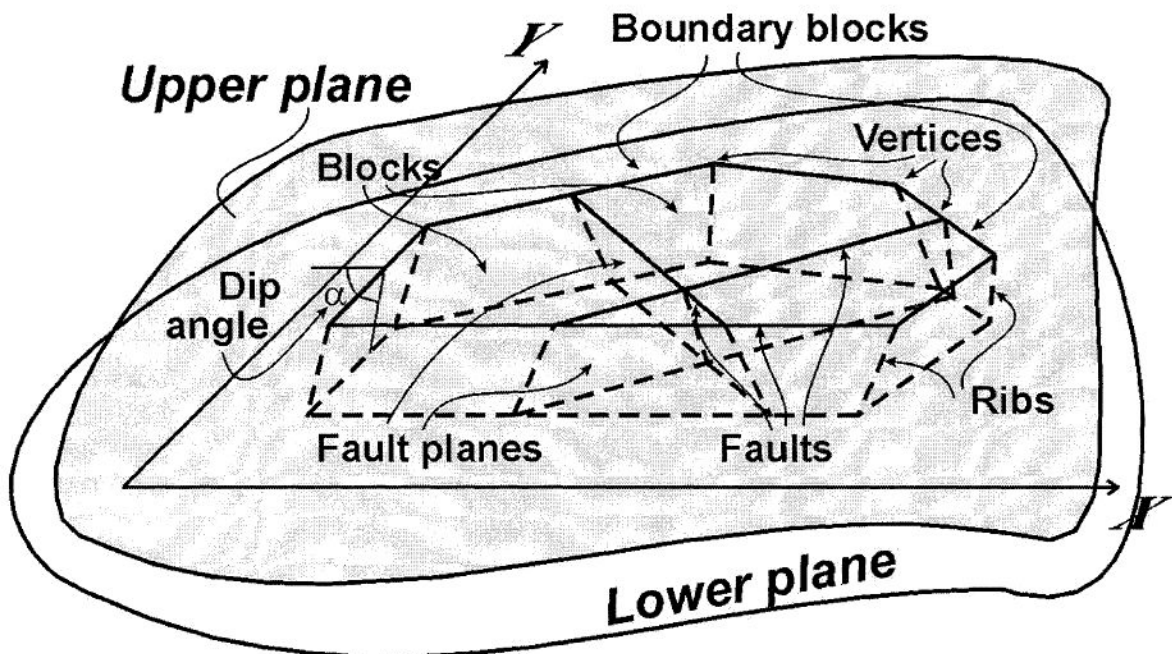


FIGURE 2 A sketch of the block-and-fault dynamics model.

2.2 Block Movement

The blocks are assumed to be rigid and all their relative displacements take place along the bounding fault planes. The interaction of the blocks with the underlying medium takes place along the lower plane, any kind of slip being possible.

The movements of the boundaries of the block structure (the boundary blocks) and the medium underlying the blocks are assumed to be an external force on the structure. The rates of these movements are considered to be horizontal and known.

Non-dimensional time is used in the model, therefore all quantities that contain time in their dimensions are referred to one unit of the non-dimensional time, and their dimensions do not contain time. For example, in the model, velocities are measured in units of length and the velocity of 5 cm means 5 cm for one unit of the non-dimensional time. When interpreting the results a realistic value is given to one unit of the non-dimensional time. For example if one unit of the non-dimensional time is one year then the velocity of 5 cm, specified for the model, means 5 cm/year.

At each time the displacements of the blocks are defined so that the structure is in a quasistatic equilibrium, and all displacements are supposed to be infinitely small, compared with the block size. Therefore the geometry of the block structure does not change during the simulation and the structure does not move as a whole.

2.3 Interaction between the Blocks and the Underlying Medium

The elastic force, which is due to the relative displacement of the block and the underlying medium, at some point of the block bottom, is assumed to be proportional to the difference between the total relative displacement vector and the vector of slippage (inelastic displacement) at the point.

The elastic force per unit area $\mathbf{f}^u = (f_x^u, f_y^u)$ applied to the point with co-ordinates (X, Y) , at some time t , is defined by

$$\begin{aligned} f_x^u &= K_u(x - x_u - (Y - Y_c)(\varphi - \varphi_u) - x_a), \\ f_y^u &= K_u(y - y_u + (X - X_c)(\varphi - \varphi_u) - y_a) \end{aligned} \quad (1)$$

where X_c and Y_c are the co-ordinates of the geometrical center of the block bottom; (x_u, y_u) and φ_u are the translation vector and the angle of rotation (following the general convention, the positive direction of rotation is anticlockwise), around the geometrical center of the block bottom, for the underlying medium at time t ; (x, y) and φ are the translation vector of the block and the angle of its rotation around the geometrical center of its bottom at time t ; (x_a, y_a) is the inelastic displacement vector at the point (X, Y) at time t .

The evolution of the inelastic displacement at the point (X, Y) is described by the equations

$$\frac{dx_a}{dt} = W_u f_x^u, \quad \frac{dy_a}{dt} = W_u f_y^u. \quad (2)$$

The coefficients K_u and W_u in (1) and (2) may be different for different blocks.

2.4 Interaction between the Blocks along the Fault Planes

At the time t , in some point (X, Y) of the fault plane separating the blocks numbered i and j (the block numbered i is on the left and that numbered j is on the right of the fault) the components Δx , Δy of the relative displacement of the blocks are defined by

$$\Delta x = x_i - x_j - (Y - Y_c^i)\varphi_i + (Y - Y_c^j)\varphi_j, \quad (3)$$

$$\Delta y = y_i - y_j + (X - X_c^i)\varphi_i - (X - X_c^j)\varphi_j$$

where X_c^i , Y_c^i , X_c^j , Y_c^j are the co-ordinates of the geometrical centers of the block bottoms, (x_i, y_i) , and (x_j, y_j) are the translation vectors of the blocks, and φ_i , φ_j are the angles of rotation of the blocks around the geometrical centers of their bottoms, at time t .

In accordance with the assumption that the relative block displacements take place only along the fault planes, the displacements along the fault plane are connected with the horizontal relative displacement by

$$\Delta_t = e_x \Delta x + e_y \Delta y, \quad (4)$$

$$\Delta_l = \Delta_n / \cos \alpha, \quad \Delta_n = e_x \Delta y - e_y \Delta x.$$

Here Δ_t and Δ_l are the displacements along the fault plane parallel (Δ_t) and normal (Δ_l) to the fault line on the upper plane; (e_x, e_y) is the unit vector along the fault line on the upper plane; α is the dip angle of the fault plane; and Δ_n is the horizontal displacement, normal to the fault line on the upper plane. It follows from (4) that Δ_n is the projection of Δ_l on the horizontal plane (Fig. 3a).

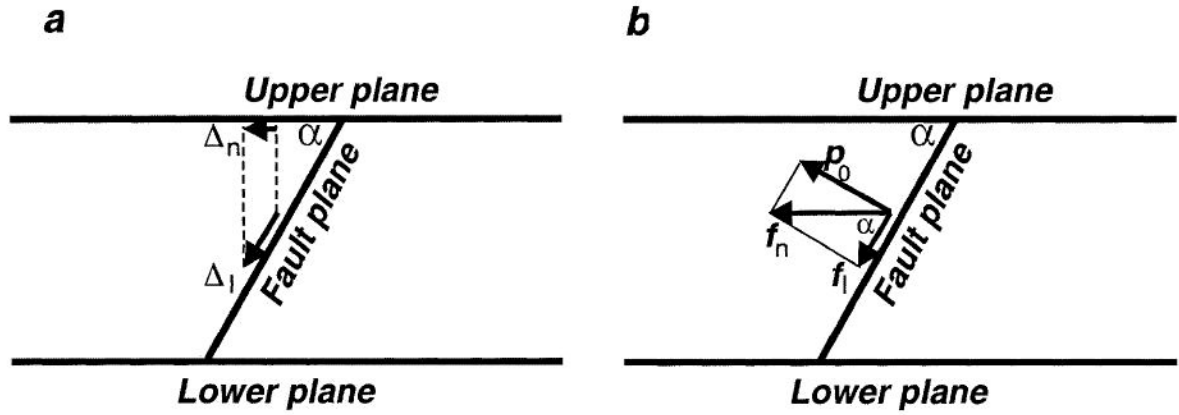


FIGURE 2 Vertical section of a block structure orthogonal to a fault. Relative displacements of blocks Δ_n and Δ_l (a) and forces p_0 , f_l , and f_n (b).

The elastic force per unit area $\mathbf{f} = (f_l, f_n)$ acting along the fault plane at the point (X, Y) is defined by

$$f_l = K(\Delta_t - \delta_t), \quad (5)$$

$$f_n = K(\Delta_l - \delta_l).$$

Here δ_t , δ_l are inelastic displacements along the fault plane at the point (X,Y) at time t , parallel (δ_t) and normal (δ_l) to the fault line on the upper plane.

The evolution of the inelastic displacement at the point (X,Y) is described by the equations

$$\frac{d\delta_t}{dt} = Wf_t, \quad \frac{d\delta_l}{dt} = Wf_l. \quad (6)$$

The coefficients K and W in (5) and (6) may be different for different faults. The coefficient K can be considered as the shear modulus of the fault plane.

Equations (5-6) correspond to visco-elastic (Maxwell) rheological law that describes the relation of \mathbf{f} to the strain ζ

$$\left(\frac{d}{dt} + \frac{1}{\tau} \right) \mathbf{f} = \mu \frac{d\zeta}{dt} \quad (7)$$

where τ is the relaxation time ($\tau = \eta / \mu$), μ is the shear modulus, and η is the viscosity. Coefficients in (5-7) are connected by formulas: $K = \mu / a$, $W = a / \eta$, a is the actual width of the fault zone; and $\tau = 1 / (KW)$.

In addition to the elastic force, there is the reaction force which is normal to the fault plane; the work done by this force is zero, because all relative movements are tangent to the fault plane. The elastic energy per unit area at the point (X,Y) is equal to

$$e = (f_t(\Delta_t - \delta_t) + f_l(\Delta_l - \delta_l)) / 2. \quad (8)$$

From (4) and (8) the horizontal component of the elastic force per unit area, normal to the fault line on the upper plane, f_n can be written as:

$$f_n = \frac{\partial e}{\partial \Delta_n} = \frac{f_l}{\cos \alpha}. \quad (9)$$

It follows from (9) that the total force acting at the point of the fault plane is horizontal if there is a reaction force, which is normal to the fault plane (Fig. 3b). The reaction force per unit area is equal to

$$p_0 = f_l \operatorname{tg} \alpha. \quad (10)$$

The reaction force (10) is introduced and therefore there are not vertical components of forces acting on the blocks and there are not vertical displacements of blocks.

Formulas (3) are also valid for boundary faults. In this case one of blocks separated by the fault is a boundary block. The movement of blocks is prescribed by their translation and rotation around the origin of co-ordinates. Therefore the co-ordinates of the geometrical center of the block bottom in (3) are set to zero for any boundary block. For example, if the block numbered j is a boundary block, then $X_c^j = Y_c^j = 0$ in (3).

2.5 Equilibrium Equations

The components of the translation vectors of the blocks and the angles of their rotation around the geometrical centers of the bottoms are found from the condition that the total force and the total moment of forces acting on each block are equal to zero. This is the condition of quasi-

static equilibrium of the system and the condition of minimum energy at the same time. The forces arising from the specified movements of the underlying medium and of the boundaries of the block structure are considered only in the equilibrium equations. In fact it is assumed that the action of all other forces (gravity, etc.) on the block structure is balanced and does not cause displacements of the blocks.

In accordance with formulas (1), (3-5), (8), and (9) the dependence of the forces, acting on the blocks, on the translation vectors of the blocks and the angles of their rotations is linear. Therefore the system of equations which describes the equilibrium is linear one and has the following form

$$Az = \mathbf{b} \quad (11)$$

where the components of the unknown vector $\mathbf{z} = (z_1, z_2, \dots, z_{3n})$ are the components of the translation vectors of the blocks and the angles of their rotation around the geometrical centers of the bottoms (n is the number of blocks), i.e. $z_{3m-2} = x_m$, $z_{3m-1} = y_m$, $z_{3m} = \varphi_m$ (m is the number of the block, $m = 1, 2, \dots, n$).

The matrix A does not depend on time and its elements are defined from formulas (1), (3-5), (9), and (10). The moment of the forces acting on a block is calculated relative to the geometrical center of its bottom. The expressions for the elements of the matrix A contain integrals over the surfaces of the fault segments and of the block bottoms. Each integral is replaced by a finite sum, in accordance with the space discretization described in Section 2.6.

The components of the vector \mathbf{b} are defined from formulas (1), (3-5), (9), and (10) as well. They depend on time, explicitly, because of the movements of the underlying medium and of the block structure boundaries and, implicitly, because of the inelastic displacements.

2.6 Discretization

Time is discretized with a step Δt . The state of the block structure is considered at discrete values of time $t_i = t_0 + i\Delta t$ ($i = 1, 2, \dots$), where t_0 is the initial time. The transition from the state at t_i to the state at t_{i+1} is made as follows:

- (i) new values of the inelastic displacements $x_a, y_a, \delta_t, \delta_l$ are calculated from equations (2) and (6);
- (ii) the translation vectors and the rotation angles at t_{i+1} are calculated for the boundary blocks and the underlying medium;
- (iii) the components of vector \mathbf{b} in equations (11) are calculated, and these equations are used to define the translation vectors and the angles of rotation for the blocks. Since the elements of A in (11) are not functions of time, the matrix A and the associated inverse matrix can be calculated only once, at the beginning of the calculation.

Formulas (1-6, 8-10) describe the forces, the relative displacements, and the inelastic displacements at points of the fault segments and of the block bottoms. Therefore the discretization of these surfaces is required for the numerical simulation. The space discretization is defined by the parameter ϵ , and it is applied to the surfaces of the fault segments and to the block bottoms. The discretization of a fault segment is performed as follows. Each fault segment is a trapezium with bases a and b and height $h = H/\sin\alpha$, where H is the thickness of the layer, and α is the dip angle of the fault plane. The values

$$n_1 = \text{ENTIRE}(h/\epsilon) + 1, \text{ and } n_2 = \text{ENTIRE}(\max(a,b)/\epsilon) + 1,$$

are defined, and the trapezium is divided into $n_1 n_2$ small trapeziums by two groups of segments inside it: $n_1 - 1$ segments, parallel to the trapezium bases and spaced at intervals h/n_1 , and $n_2 - 1$ segments connecting the points spaced by intervals of a/n_2 and b/n_2 , respectively, on

the two bases. The small trapeziums obtained in such a way are called "cells". The co-ordinates X, Y in (3) and the inelastic displacements δ_t, δ_l in (5) are supposed to be the same for all the points of a cell. These values of the co-ordinates and the inelastic displacements are considered as the average values over the cell. When introduced in formulas (3-5), (9), and (10) they yield the average over the cell of the elastic and reaction forces per unit area. The forces acting on the cell are obtained by multiplying the average forces per unit area by the area of the cell.

The bottom of a block is a polygon. Before discretization it is divided into trapeziums (triangles) by segments passing through its vertices and parallel to the Y axis. The discretization of these trapeziums (triangles) is performed in the same way as in the case of the fault segments. The small trapeziums (triangles) are also called "cells". For all the points of a cell the co-ordinates X, Y and the inelastic displacements x_a, y_a in (1) are assumed to be the same.

2.7 Earthquake and Creep

Let us introduce the quantity

$$\kappa = \frac{|\mathbf{f}|}{P - p_0} \quad (12)$$

where $\mathbf{f} = (f_t, f_l)$ is the vector of the elastic force per unit area given by (5), P is assumed equal for all the faults and can be interpreted as the difference between the lithostatic and the hydrostatic pressure, p_0 , given by (10), is the reaction force per unit area.

For each fault the following three values of κ are considered

$$B > H_f \geq H_s.$$

Let us assume that the initial conditions for the numerical simulation of block structure dynamics satisfy the inequality $\kappa < B$ for all the cells of the fault segments. If, at some time t_i , the value of κ in any cell of a fault segment reaches the level B , a failure ("earthquake") occurs. The failure is meant as slippage during which the inelastic displacements δ_t, δ_l in the cell change abruptly to reduce the value of κ to the level H_f . Thus, the earthquakes occur in accordance with the dry friction model.

The new values of the inelastic displacements in the cell are calculated from

$$\delta_t^e = \delta_t + \gamma f_t, \quad \delta_l^e = \delta_l + \gamma f_l \quad (13)$$

where $\delta_t, \delta_l, f_t, f_l$ are the inelastic displacements and the components of the elastic force vector per unit area just before the failure. The coefficient γ is given by

$$\gamma = 1/K - PH_f/(K(|\mathbf{f}| + H_f \text{tg}\alpha)). \quad (14)$$

It follows from (5), (10), and (12-14) that on obtaining the new values of the inelastic displacements the value of κ in the cell becomes equal to H_f .

After calculating the new values of the inelastic displacements for all the failed cells, the new components of the vector \mathbf{b} are calculated, and from the system of equations (11) the translation vectors and the angles of rotation for the blocks are found. If for some cell(s) of the fault segments $\kappa > B$, the procedure given above is repeated for this cell (or cells). Otherwise the state of the block structure at the time t_{i+1} is determined as follows: the translation vectors, the rotation angles (at t_{i+1}) for the boundary blocks and for the underlying medium, and the components of \mathbf{b} in equations (11) are calculated, and then equations (11) are solved.

The cells of the same fault plane where failure occurs at the same time form a single earthquake. The parameters of the earthquake are defined as follows:

- (i) the origin time is t_i ;
- (ii) the epicentral co-ordinates and the source depth are the weighted sums of the co-ordinates and depths of the cells included in the earthquake (the weight of

each cell is given by its square divided by the sum of squares of all the cells included in the earthquake);

(iii) the magnitude is calculated from

$$M = 0.98 \lg S + 3.93, \quad (15)$$

where S is the sum of the squares of the cells (in km^2) included in the earthquake and the values of coefficients are specified in accordance with *Utsu and Seki* (1954).

It is assumed that the cells, in which a failure has occurred, are in the creep state immediately after the earthquake. It means that the parameter W_s ($W_s > W$) is used instead of W for these cells in (6) describing the evolution of inelastic displacements; W_s may be different for different fault planes. After each earthquake a cell is in the creep state as long as $\kappa > H_s$, whereas when $\kappa \leq H_s$, the cell returns to the normal state and henceforth the parameter W is used in (6) for this cell.

III. CRUSTAL BLOCK-AND-FAULT DYNAMICS, FAULT SLIP RATES AND EARTHQUAKE FLOW IN THE TIBET-HIMALAYAN REGION

3.1 Block-and-Fault Structure for Tibet-Himalayan Region

Six major geological structural elements of the region (crustal blocks 1 to 6) delineated by faults (solid lines) compose the core structure of the block model (Figs. 1, 4). To avoid the determination of conditions at rigid immobile lateral boundaries of the structure (to the west, north and east of blocks 1 to 6), six additional blocks 7 to 12 are introduced in the model as boundary blocks (Fig. 4). Segments of the boundary blocks S11, S24–S38, S42, S44, S50, S62, and S63 (dashed lines) do not correspond to real geological structures, and hence $K = 0$ is specified for the segments. Therefore, according to (5), all forces and stress in these fault segments are equal to zero.

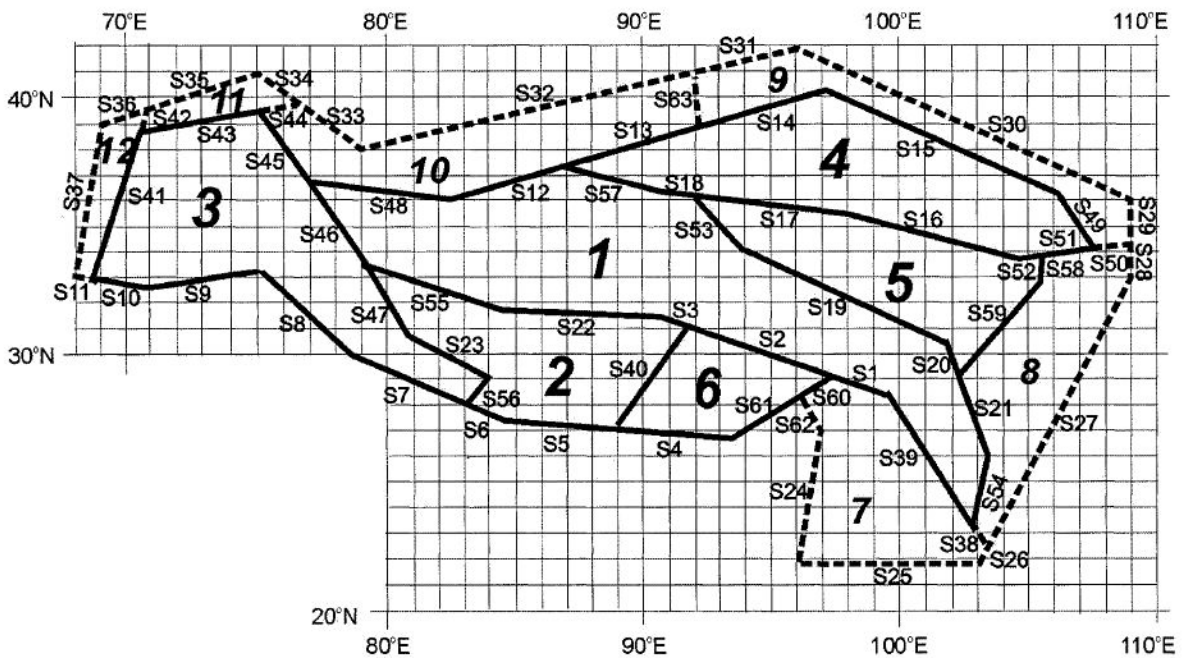


FIGURE 4 Block-and-fault structure of the Tibet-Himalayan region. Solid and dashed lines delineate blocks 1 to 6 (structural geological elements) and blocks 7 to 12 (the model boundary), respectively. S1–S63 are the fault segments.

The model structure contains 41 fault planes and 12 blocks in total. The fault planes consist of 63 segments. Dip angles of the fault planes are given in Table 1. The shallow nature of earthquake foci suggests that the upper crust is thin and underlain by a low-viscosity layer (Mazek *et al.*, 1994). We consider that an average thickness of the rigid crustal block is 30 km, and assign $H = 30$ km between the upper and lower planes (boundaries) of the model structure.

The following model parameters are specified for the blocks and the faults in our numerical experiments assuming that one unit of dimensionless time used in the model equals to one year. We prescribe $K_u = 1$ (measured in 10^7 Pa m⁻¹) and $W_u = 0.05$ (measured in 10^{-7} m Pa⁻¹ yr⁻¹) for the bottom plane of blocks 1–6 ($\tau = 20$ yr). The values of these coefficients for blocks 7–12 are varied. For fault segments S1–S10, S12–S23, S39–S41, S43, S45–S49, S51–S61, $K = 1$ and $W = 0.01$, the thresholds for κ are $B = 0.1$, $H_f = 0.085$, $H_s = 0.07$, and $W_s = 2$

(measured in 10^{-7} m Pa $^{-1}$ yr $^{-1}$). The values of the parameters for the time and space discretization are $\Delta t = 10^{-3}$ yr and $\epsilon = 16$ km, respectively. $P = 2 \cdot 10^8$ Pa in (12). The values of the parameters specified here are default values in all numerical experiments (if another values of the parameters are not prescribed).

TABLE 1 Dip angles of the fault planes in the BAFD model

#	Fault segments	Direction of fault plane slope	Dip angle
1	S1, S2, S3	S-W	85°
2	S4, S5	N	30°
3	S40	E-S	85°
4	S6, S7	N-E	30°
5	S8	N-E	30°
6	S9	N	30°
7	S10, S11	N	30°
8	S41, S42	W-N	85°
9	S43, S44	S-E	40°
10	S45, S46, S47	E-N	85°
11	S48	S	40°
12	S12, S13, S14	S-E	60°
13	S15	S-W	30°
14	S49	N-E	85°
15	S50, S51, S52	S	85°
16	S16	S-W	40°
17	S17, S18	S	40°
18	S53	N-E	85°
19	S19	N-E	85°
20	S20, S21	E-N	85°
21	S54	E	85°
22	S38, S39	S-W	85°
23	S22	S	85°
24	S55	S-W	85°
25	S56	W-N	85°
26	S23	S-W	85°
27	S57	S-W	85°
28	S58	E	85°
29	S59	E-S	85°
30	S60, S61	N-W	30°
31	S62	E-N	85°
32	S24	E-S	85°
33	S25	N	85°
34	S26, S27	W-N	85°
35	S28, S29	W	85°
36	S30	S-W	85°
37	S31, S32	S-E	85°
38	S33, S34	S-W	85°
39	S35, S36	S-E	85°
40	S37	E-S	85°
41	S63	W	85°

The movement of the model structure (with the rate of $V_x = 10 \text{ mm yr}^{-1}$, $V_y = 40 \text{ mm yr}^{-1}$) is specified for the boundary formed by segments S4 – S10, and S61. The rate is constrained by the present rate of convergence between India and Asia (Bilham *et al.*, 1997). All other parts of the lateral boundary of the structure and the medium underlying all the blocks do not move. Therefore, the movement of India plate is specified as boundary movements in the model.

The numerical simulations were performed for 4000 years starting from zero initial conditions. The total displacements of the blocks are represented in the model as their displacements along X and Y axes of the reference coordinate system and the angles of rotation around their geometrical centers. The point with the geographic coordinates 30.0°N and 90.0°E is chosen as the origin of the reference coordinate system (Fig. 4). The X axis is the east-oriented parallel passing through the origin of the coordinate system. The Y axis is the north-oriented meridian passing through the origin of the coordinate system.

3.2 Numerical Results

Five sets of numerical experiments have been performed to study the dynamics of the block-and-fault structure, seismic flow, and fault slip rates in the Tibet-Himalayan region.

3.2.1. Effect of the model boundary resistance on the block displacement rates

In *set 1* of the experiments different values of coefficients K and W for boundary blocks 7-12 are specified: $K_u = 1$, $W_u = 0.05$ (experiment 1.1); $K_u = 5$, $W_u = 0.01$ (1.2); $K_u = 20$, $W_u = 0.0025$ (1.3); $K_u = 100$, $W_u = 0.0005$ (1.4); and $K_u = 500$, $W_u = 0.0001$ (1.5). The increase in the shear modulus and viscosity of the lower crust from experiment 1.1 to 1.5 (keeping the relaxation time equal to 20 yr) results in a stronger resistance of the model boundary (blocks 7-12) with respect to the movements of blocks 1-6.

The average values of displacement rates along X and Y axes and angular velocities predicted by these numerical experiments for blocks 1-6 are shown in Table 2. Blocks 1, 2, and 4–6 rotate clockwise, and block 3 rotates clockwise in experiments 1.1 and 1.2 and counterclockwise in experiments 1.4 and 1.5. When the GPS data are viewed in a fixed Eurasian frame of reference (Abdrakhmatov *et al.*, 1996; Chen *et al.*, 2000; Shen *et al.*, 2000; Wang *et al.*, 2001; Burchfiel, 2004), the central and eastern parts of the region (corresponding to blocks 1, 2, 4–6 in the BAFD model) move east-southeast and the western part of the region (corresponding to block 3) tends to move north-northwest related to Siberia. These observations are consistent with the model predictions on the displacement rates of the crustal blocks.

Synthetic earthquakes occur on segments S4 – S10, and S61 in all experiments and also on segment S1 in experiments 1.4 and 1.5. The plots of cumulative number (on a logarithmic scale) of earthquakes with magnitudes greater than M as a function of magnitude M (hereinafter we refer to it as *FM plots*) for synthetic seismicity obtained in *set 1* of the experiments are presented in Fig. 5a. The seismicity generated by the model experiments is associated with the fault system in the Himalayan Frontal Thrust. It is rather natural, because Himalayas is a part of the region with the highest level of observed seismic activity. The FM plot for the observed seismicity is also shown in Fig. 5a (dashed line). If the slopes of the FM plots for the observed and synthetic seismicity are compared, we see that the results of experiment 1.3 give the closest fit to the slope of the observed seismicity. The values of the model parameters specified in experiment 1.3 are used as a benchmark in other sets of numerical experiments with the BAFD model.

The increase of the shear modulus and viscosity of the lower crust beneath the model boundary makes this portion of the crust more resistant to the regional motion, and hence the displacement rates of the blocks and hence slip rates at the faults separating the blocks are

diminishing. In experiment 1.1 the maximum displacement rates of blocks 2 and 3 (separated by the Karakorum fault) are about 15 mm yr^{-1} and 8 mm yr^{-1} , respectively (Fig. 6a). The rates drop to about 3 mm yr^{-1} at these blocks in experiment 1.5 and to even less values (about 1 mm yr^{-1}) for another blocks.

TABLE 2 Displacement rates (V_x , V_y) and angular velocities of blocks 1-6 predicted by *set 1* of numerical experiments

Experiment	Number of synthetic earthquakes and range of their magnitudes	Segments where earthquakes occurred	Block	V_x , cm	V_y , cm	Angular velocity, 10^{-6} rad
1.1	86002 $6.19 \leq M \leq 7.30$	S4-S10, S61	1	0.10418	0.38556	-0.00256
			2	1.39496	0.54002	-0.00259
			3	0.14132	0.81865	-0.00214
			4	0.13327	0.22195	-0.00286
			5	0.12490	0.17154	-0.00260
			6	0.01515	0.38304	-0.00291
1.2	81775 $6.19 \leq M \leq 8.30$	S4-S10, S61	1	0.05711	0.28969	-0.00176
			2	0.01687	0.40696	-0.00179
			3	0.05784	0.58768	-0.00092
			4	0.08871	0.16063	-0.00203
			5	0.08016	0.13298	-0.00185
			6	-0.00272	0.30110	-0.00216
1.3	54056 $6.19 \leq M \leq 8.28$	S4-S10, S61	1	0.03344	0.22608	-0.00131
			2	0.01608	0.31971	-0.00127
			3	0.02122	0.42374	0.00000
			4	0.05730	0.12162	-0.00159
			5	0.05452	0.10424	-0.00141
			6	-0.00065	0.24148	-0.00170
1.4	79619 $6.18 \leq M \leq 7.65$	S1, S4-S10, S61	1	0.03581	0.17800	-0.00110
			2	0.04700	0.25639	-0.00095
			3	0.03442	0.29689	0.00066
			4	0.04125	0.09752	-0.00130
			5	0.04325	0.08254	-0.00116
			6	0.02725	0.18943	-0.00144
1.5	91241 $6.18 \leq M \leq 7.48$	S1, S4-S10, S61	1	0.04155	0.15956	-0.00104
			2	0.06713	0.23225	-0.00083
			3	0.04993	0.24558	0.00092
			4	0.03639	0.08988	-0.00120
			5	0.04018	0.07492	-0.00108
			6	0.04495	0.16765	-0.00134

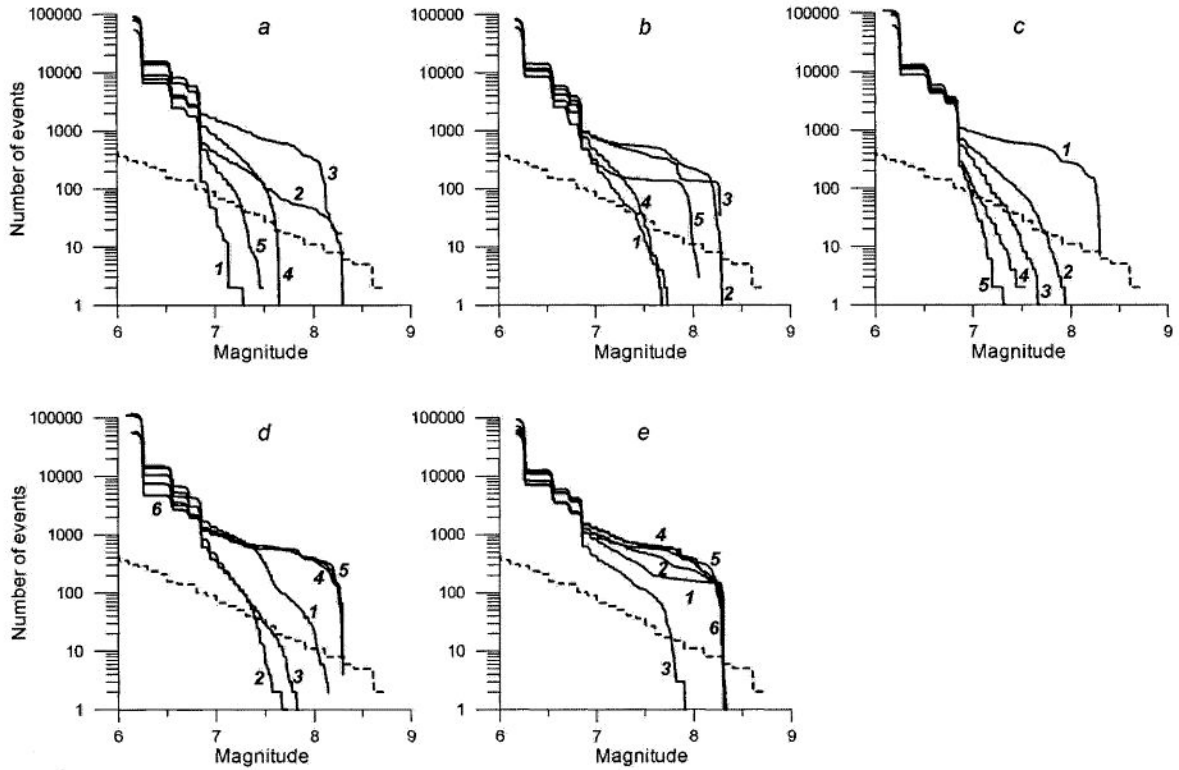


FIGURE 5 Cumulated FM plots for synthetic seismicity (solid lines) predicted by numerical experiments: (a) set 1 to (e) set 5. Solid lines marked by k ($k=1, 2, 3, 4, 5$, and 6) present the number of the experiment in set i ($i=1, 2, 3, 4$, and 5). The cumulated FM plot for the observed seismicity from 1967 to 2003 is shown by a dashed line.

3.2.2. Variations in the movement of the Indian plate with respect to Eurasia

In *set 2* of experiments we analyze how the direction of the Indian plate motion with respect to Eurasia influences the seismicity and displacement rates of blocks 1 to 6. The direction of this motion changes from the north to the northeast; the rotation angle with the meridian changes from 0° to 40° (each 10°) with experiments 2.1 to 2.5. We specify the following velocity (V_x, V_y) of the motion at segments S4 – S10, and S61: $V_x = 0, V_y = 40 \text{ mm yr}^{-1}$ (experiment 2.1); $V_x = 6.946, V_y = 39.392$ (2.2); $V_x = 13.681, V_y = 37.588$ (2.3); $V_x = 20, V_y = 34.641$ (2.4); and $V_x = 25.712, V_y = 30.642$ (2.5). We keep the magnitude of the displacement rate to be 40 mm yr^{-1} . Values of all other model parameters are the same as in experiment 1.3.

The average values of the displacement rates along X and Y axes and angular velocities obtained in these experiments are shown for blocks 1-6 in Table 3. In all experiments of set 2, blocks 1, 2, 4–6 rotate clockwise, block 3 rotates clockwise in experiments 2.1 and 2.2 and counterclockwise in other experiments. Also in all experiments, synthetic earthquakes occur on segments S4–S10, and S61. Cumulated FM plots for the synthetic seismicity obtained in this set of experiments as well as that for the observed seismicity are presented in Fig. 5b. The slope of the FM plot for the observed earthquakes is the closest to the slope of the FM plot for synthetic seismicity generated in experiment 2.3. The numerical experiments show that the change in the direction of the Indian plate motion affects mainly the displacement rates of block 3 (Fig. 6b). The rates of the displacement of another blocks vary slightly.

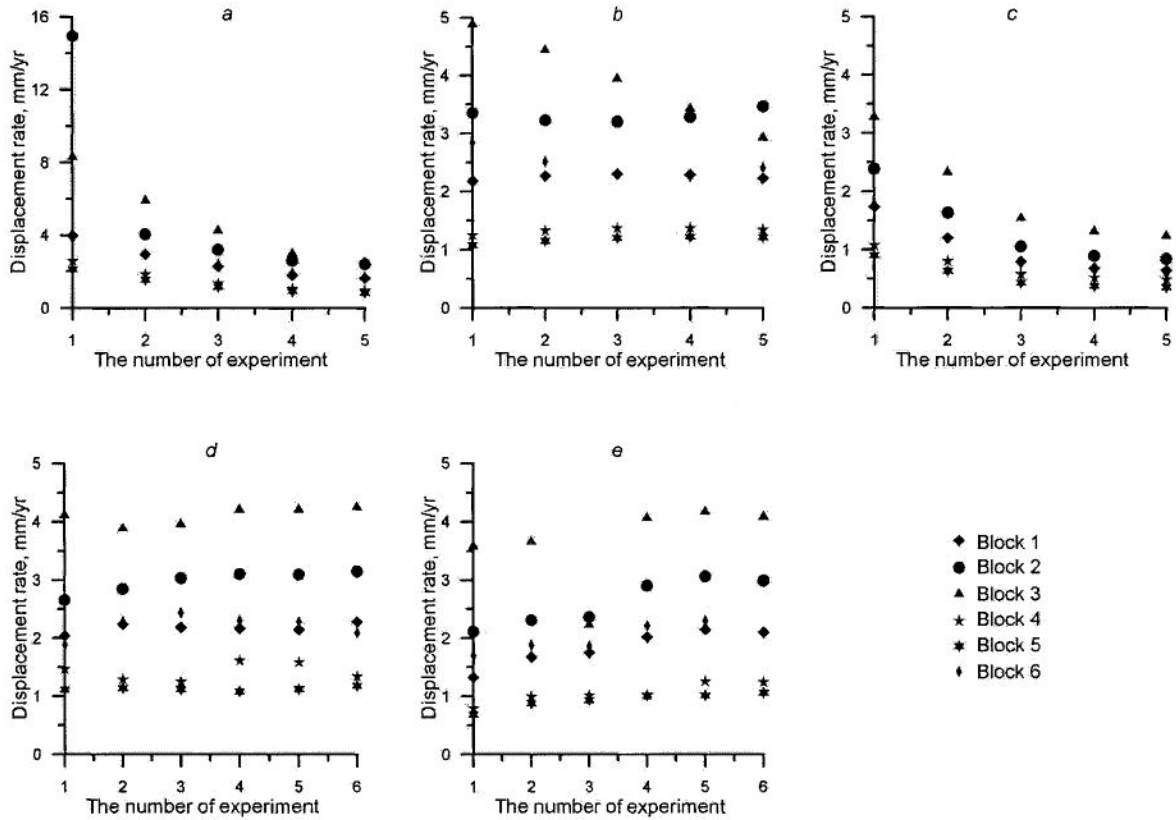


FIGURE 6 Displacement Rates for each crustal block in the numerical experiments: (a) set 1 to (e) set 5.

3.2.3. Effects of the elastic properties and viscosity of fault zones on slip rates

In set 3 of experiments the values of coefficients K , W , and W_s vary at internal fault segments (S1 – S3, S12 – S23, S39 – S41, S43, S45 – S49, and S51 – S60) with the nonzero shear modulus: $K = 2$, $W = 0.005$, $W_s = 1$ (experiment 3.1); $K = 5$, $W = 0.002$, $W_s = 0.4$ (3.2); $K = 20$, $W = 0.0005$, $W_s = 0.1$ (3.3); $K = 50$, $W = 0.0002$, $W_s = 0.04$ (3.4); and $K = 100$, $W = 0.0001$, $W_s = 0.02$ (3.5). The changes of the parameters result in an increase of the shear modulus and viscosity of the relevant fault zones from experiment 3.1 to 3.5. Values of all other model parameters are the same as in experiment 1.3.

The average values of the displacement rates along X and Y axes and angular velocities obtained in these experiments are shown for blocks 1-6 in Table 4. In all experiments of this set blocks 1 – 6 rotate clockwise. In these experiments synthetic earthquakes occur on segments S4 – S10, S61, S46, and S56. Cumulated FM plots for synthetic seismicity obtained in set 3 of the experiments are presented in Fig. 5c. The slopes of the FM plots for these experiments (besides experiment 3.1) differ essentially from the slope of the FM plot for the observed seismicity. The number of large events decreases as the resistance of fault planes to slip increases with the shear modulus and viscosity. In experiment 3.1 the maximum displacement rates of blocks 2 and 3 are about 2.5 and 3.3 mm yr⁻¹, respectively (Fig. 6a). The rates decrease to about 1 and 1.3 mm yr⁻¹ at these blocks in experiment 3.5 and to even less values (about 0.3 mm yr⁻¹) for another blocks.

TABLE 3 Displacement rates (V_x , V_y) and angular velocities of blocks 1-6 predicted by *set 2* of numerical experiments

Experiment	Number of synthetic earthquakes and range of their magnitudes	Segments where earthquakes occurred	Block	V_x , cm	V_y , cm	Angular velocity, 10^{-6} rad
2.1	83018 $6.19 \leq M \leq 7.75$	S4-S10, S61	1	0.01118	0.21802	-0.00117
			2	-0.09283	0.32229	-0.00150
			3	-0.04491	0.48629	-0.00095
			4	0.05053	0.11452	-0.00129
			5	0.04178	0.10006	-0.00260
			6	-0.09748	0.26717	-0.00185
2.2	59260 $6.19 \leq M \leq 8.30$	S4-S10, S61	1	0.02730	0.22505	-0.00128
			2	-0.01488	0.32226	-0.00135
			3	0.00252	0.44397	-0.00027
			4	0.05570	0.12028	-0.00156
			5	0.05119	0.10363	-0.00138
			6	-0.02832	0.25015	-0.00176
2.3	58978 $6.19 \leq M \leq 8.28$	S4-S10, S61	1	0.04243	0.22632	-0.00135
			2	0.06248	0.31403	-0.00116
			3	0.04906	0.39102	0.00041
			4	0.05936	0.12293	-0.00162
			5	0.05917	0.10456	-0.00144
			6	0.04093	0.22705	-0.00162
2.4	82495 $6.19 \leq M \leq 7.68$	S4-S10, S61	1	0.05648	0.22202	-0.00139
			2	0.13842	0.29806	-0.00094
			3	0.09418	0.32880	0.00107
			4	0.06156	0.12255	-0.00164
			5	0.06567	0.10293	-0.00146
			6	0.10941	0.19829	-0.00144
2.5	79412 $6.19 \leq M \leq 8.06$	S4-S10, S61	1	0.06929	0.21210	-0.00140
			2	0.21178	0.27446	-0.00069
			3	0.13724	0.25832	0.00171
			4	0.06225	0.11908	-0.00161
			5	0.07059	0.09866	-0.00145
			6	0.17603	0.16411	-0.00124

3.2.4. Strong versus weak resistance to block displacement

In *set 4* of experiments we analyze the influence of resistance to displacement of an individual crustal block on seismicity and block displacement rates. Values $K = 100$, $W = 0.0001$ (higher shear modulus and viscosity compared to default ones), and $W_s = 0.02$ are assigned to the fault segments bounding blocks 1 to 6 (besides those that form the model boundary, where the movement is specified, and those adjacent to blocks 7–12), namely: to segments S2, S3, S18–S20, S22, S46, S53, S55, and S57 bounding block 1 (in experiment 4.1); to segments S3, S22, S23, S40, S47, S55, and S56 bounding block 2 (in 4.2); to segments S23, S46, S47, and S56 bounding block 3 (in 4.3); to segments S16–S18, S52, and S57 bounding block 4 (in 4.4); to segments S16, S17, S19, S20, S52, and S53 bounding block 5 (in 4.5); and to segments S2 and S40 bounding block 6 (in 4.6). Values of all other model parameters are the same as in experiment 1.3.

TABLE 4 Displacement rates (V_x , V_y) and angular velocities of blocks 1-6 predicted by set 3 of numerical experiments

Experiment	Number of synthetic earthquakes and range of their magnitudes	Segments where earthquakes occurred	Block	V_x , cm	V_y , cm	Angular velocity, 10^{-6} rad
3.1	61907 $6.19 \leq M \leq 8.30$	S4-S10, S61	1	0.02168	0.17204	-0.00098
			2	-0.00252	0.23880	-0.00099
			3	0.01492	0.32753	-0.00033
			4	0.04972	0.09493	-0.00116
			5	0.03966	0.08089	-0.00105
			6	-0.01422	0.17843	-0.00121
3.2	94701 $6.18 \leq M \leq 7.95$	S1, S4-S10, S61	1	0.01499	0.11937	-0.00069
			2	-0.00726	0.16318	-0.00072
			3	0.01561	0.23282	-0.00047
			4	0.04108	0.06887	-0.00077
			5	0.02610	0.05772	-0.00072
			6	-0.01521	0.11974	-0.00080
3.3	105478 $6.18 \leq M \leq 7.67$	S1, S4-S10, S46, S61	1	0.01137	0.07844	-0.00047
			2	-0.00281	0.10517	-0.00048
			3	0.01808	0.15307	-0.00043
			4	0.03122	0.04844	-0.00049
			5	0.01628	0.03940	-0.00048
			6	-0.00866	0.07479	-0.00050
3.4	110120 $6.10 \leq M \leq 7.52$	S1, S4-S10, S56, S61	1	0.01018	0.06754	-0.00040
			2	-0.00101	0.08966	-0.00041
			3	0.01821	0.13034	-0.00039
			4	0.02788	0.04292	-0.00041
			5	0.01361	0.03455	-0.00041
			6	-0.00635	0.06301	-0.00042
3.5	109808 $6.10 \leq M \leq 7.33$	S1, S4-S10, S56, S61	1	0.00963	0.06359	-0.00038
			2	-0.00039	0.08399	-0.00038
			3	0.01807	0.12184	-0.00038
			4	0.02666	0.04090	-0.00038
			5	0.01258	0.03282	-0.00038
			6	-0.00554	0.05876	-0.00039

The average rates of displacements along X and Y axes and angular velocities obtained in these experiments are shown for blocks 1-6 in Table 5. In all experiments of set 4 of the numerical experiments, blocks 1 – 6 rotate clockwise. In these experiments synthetic earthquakes occurred on segments S4 – S10, S61, S23, S40, S46, S47, S56, and S57. Cumulated FM plots for seismic events (predicted by these experiments and observed) are presented in Fig. 5d. The slopes of the plots for experiments 4.4 – 4.6 are rather close to the slope of the plot for observed seismicity. The numerical experiments show also that displacement rates of the crustal blocks vary with the rheological parameters of the fault segments.

TABLE 5 Displacement rates (V_x , V_y) and angular velocities of blocks 1-6 predicted by *set 4* of numerical experiments

Experiment	Number of synthetic earthquakes and range of their magnitudes	Segments where earthquakes occurred	Block	V_x , cm	V_y , cm	Angular velocity, 10^{-6} rad
4.1	116972 $6.15 \leq M \leq 8.14$	S4-S10, S46, S57, S61	1	0.02211	0.20310	-0.00119
			2	-0.00576	0.26531	-0.00119
			3	0.02984	0.40995	-0.00073
			4	0.07350	0.12763	-0.00129
			5	0.03084	0.10746	-0.00119
			6	-0.02621	0.18740	-0.00120
4.2	110121 $6.10 \leq M \leq 7.72$	S4-S10, S23, S40, S47, S56, S61	1	0.01072	0.22434	-0.00113
			2	-0.01904	0.28410	-0.00112
			3	0.03033	0.38712	-0.00100
			4	0.05129	0.11808	-0.00147
			5	0.04466	0.10562	-0.00128
			6	-0.02354	0.22805	-0.00111
4.3	105248 $6.19 \leq M \leq 7.83$	S4-S10, S46, S47, S61	1	0.01056	0.21849	-0.00109
			2	-0.01653	0.30339	-0.00094
			3	0.02922	0.39481	-0.00092
			4	0.04991	0.11506	-0.00143
			5	0.04384	0.10325	-0.00124
			6	-0.02915	0.24272	-0.00147
4.4	55317 $6.15 \leq M \leq 8.29$	S4-S10, S57, S61	1	0.03297	0.21435	-0.00134
			2	0.01307	0.31012	-0.00131
			3	0.02047	0.42008	-0.00006
			4	0.09480	0.13076	-0.00141
			5	0.04160	0.09996	-0.00140
			6	-0.00378	0.23022	-0.00174
4.5	55000 $6.19 \leq M \leq 8.29$	S4-S10, S61	1	0.03422	0.21251	-0.00136
			2	0.01363	0.30945	-0.00133
			3	0.02153	0.42049	-0.00007
			4	0.09241	0.12969	-0.00132
			5	0.04388	0.10353	-0.00136
			6	-0.00356	0.22819	-0.00176
4.6	57808 $6.19 \leq M \leq 8.29$	S4-S10, S40, S61	1	0.03372	0.22617	-0.00130
			2	0.01033	0.31496	-0.00136
			3	0.02000	0.42470	-0.00006
			4	0.05729	0.12175	-0.00159
			5	0.05488	0.10456	-0.00141
			6	-0.01813	0.20886	-0.00134

3.2.5. Lateral variations in shear modulus and viscosity of the lower crust

In numerical experiment of *set 5* we increase the shear modulus and viscosity of the lower crust in blocks 1 to 6 one after another, that is, $K_u = 5$ and $W_u = 0.01$ are assigned to block 1 (in experiment 5.1); block 2 (in 5.2); block 3 (in 5.3); block 4 (in 5.4); block 5 (in 5.5); and block 6 (in 5.6). Values of all other model parameters are the same as in experiment 1.3.

TABLE 6 Displacement rates (V_x , V_y) and angular velocities of blocks 1-6 predicted by *set 5* of numerical experiments

Experiment	Number of synthetic earthquakes and range of their magnitudes	Segments where earthquakes occurred	Block	V_x , cm	V_y , cm	Angular velocity, 10^{-6} rad
5.1	70563 $6.19 \leq M \leq 8.34$	S4-S10, S61	1	0.02987	0.12940	-0.00083
			2	-0.02173	0.21038	-0.00105
			3	-0.00692	0.35738	-0.00062
			4	0.03695	0.07035	-0.00096
			5	0.03576	0.05837	-0.00087
			6	-0.02341	0.16889	-0.00136
5.2	61140 $6.19 \leq M \leq 8.32$	S4-S10, S61	1	0.03217	0.16475	-0.00098
			2	0.00882	0.23091	-0.00107
			3	0.01071	0.36539	-0.00036
			4	0.04396	0.08952	-0.00117
			5	0.04418	0.07661	-0.00105
			6	0.00600	0.18785	-0.00142
5.3	92081 $6.19 \leq M \leq 7.91$	S4-S10, S61	1	0.01850	0.17387	-0.00087
			2	0.04505	0.23161	-0.00058
			3	0.03504	0.22036	0.00075
			4	0.03948	0.09381	-0.00116
			5	0.04111	0.08421	-0.00099
			6	0.02809	0.18430	-0.00115
5.4	54518 $6.15 \leq M \leq 8.32$	S4-S10, S61	1	0.03116	0.19978	-0.00119
			2	0.00528	0.29031	-0.00122
			3	0.01324	0.40608	-0.00017
			4	0.03684	0.09474	-0.00141
			5	0.05007	0.08834	-0.00130
			6	-0.00767	0.22121	-0.00162
5.5	52316 $6.19 \leq M \leq 8.29$	S4-S10, S61	1	0.03082	0.21264	-0.00129
			2	0.01051	0.30627	-0.00127
			3	0.01763	0.41655	-0.00008
			4	0.05598	0.11221	-0.00153
			5	0.04836	0.08955	-0.00136
			6	-0.00527	0.22972	-0.00170
5.6	54366 $6.19 \leq M \leq 8.29$	S4-S10, S61	1	0.03579	0.20753	-0.00128
			2	0.02501	0.29817	-0.00124
			3	0.02421	0.40770	-0.00002
			4	0.05503	0.11175	-0.00150
			5	0.05105	0.09355	-0.00135
			6	0.00394	0.20906	-0.00146

The average rates of displacements along X and Y axes and angular velocities obtained in these experiments are shown for blocks 1-6 in Table 6. In all these experiments blocks 1, 2, 4-6 rotate clockwise. Block 3 rotates clockwise in all experiments besides experiment 5.3. In all experiments synthetic earthquakes occurred only on segments S4-S10, and S61. Cumulated FM plots for synthetic seismicity obtained in this set of experiments are illustrated in Fig. 5e. The slope of the plot for experiment 5.2 is the closest to that for the observed

seismicity. The numerical experiments of set 5 show that displacement rates of the crustal blocks vary with the rheological parameters of the lower crust.

3.3 Discussion

3.3.1. Slip rates

The results of numerical experiments based on the block model allow us to interpret the contemporary movement in the Tibet-Himalayan region as a motion of the rigid upper crustal blocks driven by the north-northeastward indentation of India into Eurasia. The experiments of sets 1 and 3 show that the weaker is the resistance of the lower crust and fault zones, the larger is the displacement rates of the upper crustal blocks and relative slip rates at the faults separating the blocks. The average displacement rates of the crustal blocks vary from 15 to 0.1 mm yr⁻¹ in different experiments.

Studies on major Cenozoic fault systems in the region using various techniques show that a single fault can have various slip rates at different time scales when measured by different techniques: satellite radar interferometry (InSAR) and geodetic (GPS) for a time scale of a few years; cosmogenic dating for thousands of years, and geologic measurements for millions of years. The difference in the slip rate estimates varies up to one order of magnitude, much larger than the uncertainties of each technique.

Estimates of the Holocene slip rate of the central Altyn Tagh Fault vary from 2 to 40 mm yr⁻¹ (Peltser *et al.*, 1989; Ge *et al.*, 1992). Based on radiocarbon and ¹⁰Be-²⁶Al cosmic ray exposure dating applied to determine the ages of geomorphic markers left-laterally displaced by the Altyn Tagh Fault, Meriaux *et al.* (2004) have recently estimated an average slip rate along the fault to be 26.9 (±6.9) mm yr⁻¹. Meanwhile the geodetic and satellite radar interferometry observations predict much lower slip rates than that estimated for the longer time interval. GPS measurements give a slip rate along the fault at about 10 mm yr⁻¹ (Bendick *et al.*, 2000; Chen *et al.*, 2000; Shen *et al.*, 2001). Surface displacement measurements using InSAR provide slip rates to be about 5 (±5) mm yr⁻¹ (Wright *et al.*, 2004).

Slip-rate measurements on the Karakorum Fault have come also from different sources. Based on the offsets up to thousand km for geologic markers along the fault and the age of the motion (about 30 million year) the slip rate along the fault is estimated to be about 30 mm yr⁻¹ (Peltzer and Tapponnier, 1988). However, lower slip rates of 4 to 8 mm yr⁻¹ have been also reported for the fault (Brown *et al.*, 2002; Searle *et al.*, 1998). ¹⁰Be surface exposure dating of offset moraines yields a long-term (up to 140,000 yrs) slip rate of 10.7 (±0.7) mm yr⁻¹ (Chevalier *et al.*, 2005). On the other hand, the geodetic measurements made over ten years suggest rates of 3 (±5) mm yr⁻¹ (Jade *et al.*, 2004) and 11 (±4) mm yr⁻¹ (Banerjee and Bürgmann, 2002), and the estimates based on InSAR measurements give only 1(±3) mm yr⁻¹ (Wright *et al.*, 2004).

Such a big difference in the slip-rate determinations at the major faults in the Tibetan plateau can be explained by fluctuations in rheological properties of the fault plane zones and/or the lower crust. The results of our numerical experiments based on the block model illustrate that the displacement rates of the crustal blocks (and hence the relative slip rate along the faults separating the blocks) vary with the changes of viscosity and shear modulus for the lower crust and the fault plane zones (Fig. 6a,c). This provides a possible explanation for discrepancies between the geologic estimates of the long-term fault slip rates and the slip rate estimates from geodetic and InSAR data. The rheological properties of the fault plane zones can vary with time. A change in the stress and/or fluid pressure on a cracked material of the fault zones will result in the distortion of the cracks, which will in its turn alter the effective elastic parameters of the faults zone (Hudson, 2000; Tod, 2002). Also a presence of water can greatly reduce the viscosity of the fault zones (Chopra and Paterson, 1984).

3.3.2. Earthquake flow

The numerical results demonstrate that the slope of the FM plots is also sensitive to the changes in the rheological properties of the lower crust and fault plane zones. The maximum magnitude of the events (synthetic earthquakes) at the Himalayan region increases initially with the increase in the resistance of the Tibetan crustal blocks (rise of viscosity and shear modulus of the lower crust and fault plane zones) and then decrease (see Table 2, 4 and Fig. 5a,c).

Our numerical results show also that the changes in the rheological properties of individual fault zones in the Tibetan plateau tend to promote clustering of large earthquakes. The events localize only at some of these faults (but not at all of the individual faults where the elastic and viscous coefficients were equally changed). This illustrates the fact that the block model describes dynamics of a network of the crustal blocks and the fault planes rather than dynamics of individual fault planes.

Large synthetic events in most of the numerical experiments are clustered mainly on the fault segments associated with the Himalayan Frontal Thrust where the movement is specified. In some experiments the slope of the FM plots for the synthetic events is rather close to that for observed seismicity. While the present model explains the movements and slip rates in the region well enough, there is a still unsolved problem in reproducing observed seismicity in the inner fault segments of the Tibetan plateau. A knowledge of the lower crust flow, which can be retrieved from detailed regional seismic tomography (Wittlinger *et al.*, 2004) and anisotropy models (Shapiro *et al.*, 2004) can assist in constraining the model parameters of the lower crust.

3.4 Conclusion

The block model provides a tool for studying both deformations (e.g. stress, strain, slip and slip rates) and seismicity (e.g., clustering of earthquakes, relationships between frequency and magnitude of the events, interaction between earthquakes). Based on this model we have analyzed a block-and-fault structure of the Tibet plateau and Himalayans, which incorporated major regional geological structural units and faults. Numerical experiments have addressed to better understanding dynamics of the crustal seismicity and fault slip rates in the region. The results of the research can allow us to conclude the following.

1. The present movements in the region are characterized by the north-northeastern motion of India toward Eurasia.
2. Fluctuations in rheological properties of the fault zones and/or the lower crust influence displacement rates of the crustal blocks and hence slip rates at the faults separating the blocks. This can explain the discrepancies in estimates of slip rates at major faults in the region (e.g., Altyn Tagh, Karakorum) based on different techniques (e.g., GPS, InSAR, cosmogenic dating, geological).
3. Clustering of earthquakes is a consequence of dynamics of the crustal blocks and the faults in the region. The number and the maximum magnitude of synthetic earthquakes change with variations in the movement of the crustal blocks and in the rheological properties of the lower crust and the fault zones.

Acknowledgements. The study was partially done at the Abdus Salam International Center for Theoretical Physics, (Trieste, Italy) within the framework of the SAND group activity and supported by a special grant of the French Ministry of Research.

REFERENCES

- Abdrakhmatov, K.Y. et al. (1996) Relatively recent construction of the Tien Shan inferred from GPS measurements of present day crustal deformation rate, *Nature*, 384, 450–453.
- Alekseevskaya, M. A., A. M. Gabrielov, A. D. Gvishiani, I. M. Gelfand, and E. Ya. Ranzman (1977), Formal morphostructural zoning of mountain territories, *J. Geophys.*, 43, 227–233.
- Allègre, C. J., J.-L. Le Mouél, H. D. Chau, and C. Narteau (1995), Scaling organization of fracture tectonics (SOFT) and earthquake mechanism, *Phys. Earth Planet. Inter.*, 92, 215–233.
- Armijo, R., P. Tapponnier, P., J. L. Mercier, T.-L. Han (1986), Quaternary extension in Southern Tibet: Field observations and tectonic implications, *J. Geophys. Res.*, 91(B14), 13803–13872.
- Armijo, R., P. Tapponnier, and H. Tonglin (1989), Late Cenozoic right lateral strike-slip faulting in southern Tibet, *J. Geophys. Res.*, 94(B3), 2787–2838.
- Avouac, J. P., and P. Tapponnier (1993), Kinematic model of active deformation in central-Asia, *Geophys. Res. Lett.*, 20(10), 895–898.
- Banerjee, P., and R. Bürgmann (2002), Convergence across the northwest Himalayas from GPS measurements, *Geophys. Res. Lett.*, 29(13), 1652, doi:10.1029/2002GL 015184.
- Barazangi, M., and J. Ni (1982), Velocities and propagation characteristics of Pn and Sn beneath the Himalayan arc and Tibetan plateau: possible evidence for underthrusting of Indian continental lithosphere beneath Tibet, *Geology*, 10, 179–185.
- Beaumont, C., R. A. Jamieson, M. H. Nguyen, and B. Lee (2001b), Himalayan tectonics explained by extrusion of a low-viscosity channel coupled to focused surface denudation, *Nature*, 414, 738–742.
- Bendick, R., R. Bilham, J. Freymueller, K. Larson, and G. Yin (2000), Geodetic evidence for a slip rate in the Altyn Tagh fault system, *Nature*, 404, 69–72.
- Bilham, R., K. Larson, J. Freymueller & Project Idylhim members (1997), GPS measurements of present-day convergence across the Nepal Himalayas, *Nature*, 386, 61–64.
- Bird, P. (1991), Lateral extrusion of lower crust from under high topography, in the isostatic limit, *J. Geophys. Res.*, 96, 10,275–10,286.
- Brown, E. T., R. Bendick, D. L. Bourles, V. Gaur, P. Molnar, G. M. Raisbeck, and F. Yiou (2002), Slip rates of the Karakorum fault, Ladakh, India, determined using cosmic ray exposure dating of debris flows and moraines, *J. Geophys. Res.*, 107(B9), 2192, doi:10.1029/2000JB000100.
- Burchfiel, B.C. (2004), New technology; new geological challenges, *GSA Today*, 14(2), 4–10.
- Chen, Z., Burchfiel, B.C., Liu, Y., King, R.W., Royden, L.H., Tang, W., Wang, E., Zhao, J., and W. Zhang, W. (2000), GSA measurements from eastern Tibet and their implications for India/Eurasia intracontinental deformation, *J. Geophys. Res.*, 105, 16215–16227.
- Chevalier, M. L., F. J. Ryerson, P. Tapponnier, R. C. Finkel, J. Van Der Woerd, L. Haibing, and L. Qing (2005), Slip-rape measurements on the Karakorum fault may imply secular variations in fault motion, *Science*, 307, 411–414.
- Chopra, P. N., and M. S. Paterson (1984), The role of water in the deformation of dunite, *J. Geophys. Res.*, 89, 7861–7876.
- Clark, M. K., and L. H. Royden (2000), Topographic ooze: Building the eastern margin of Tibet by lower crustal flow, *Geology*, 28, 703–706.
- England, P., and P. Molnar (1997a), Active deformation of Asia: From kinematics to dynamics, *Science*, 278, 647–650.
- England, P., and P. Molnar (1997b), The field of crustal velocity in Asia calculated from Quaternary rates of slip on faults, *Geophys. J. Int.*, 130, 551–582.

- Fielding, E., B. L. Isacks, M. Barazangi, and C. Duncan (1994), How flat is Tibet? *Geology*, 22, 163–167.
- Gabrielov, A. M., V. I. Keilis-Borok, T. A. Levshina, and V. A. Shaposhnikov (1986). Block model of dynamics of the lithosphere. In V.I. Keilis-Borok and A.L. Levshin (eds), *Mathematical Methods in Seismology and Geodynamics*. Moscow, Nauka, pp. 168-178 (*Comput. Seismol.*; Iss. 19, in Russian). English translation: *Computational Seismology*, Vol. 19, Allerton Press Inc., 1986, pp. 168-177.
- Gabrielov, A. M., T. A. Levshina, and I. M. Rotwain (1990), Block model of earthquake sequence, *Phys. Earth Planet. Inter.*, 61, 18–28.
- Gabrielov, A., and W. I. Newman (1994), Seismicity modeling and earthquake prediction: A review, In: *Nonlinear Dynamics and Predictability of Geophysical Phenomena*, W.I. Newman, A. Gabrielov, and D.L. Turcotte (Eds), pp. 7–13, Amer. Geophys. Union, Intl Union of Geodesy and Geophys., 1994 (Geophysical Monograph 83, IUGG Vol. 18).
- Gabrielov, A., I. Zaliapin, W. I. Newman, and V. I. Keilis-Borok (2000). Colliding cascades model for earthquake prediction. *Geophys. J. Int.*, 143, 2, 427- 437.
- Ge, S., G. Shen, R. Wei, G. Ding, and Y. Wang (1992), Active Altyn Fault Zone Monograph, State Seismol. Bur. of China, Beijing. 319 pp.
- Hattori, S. (1974), Regional distribution of *b*-value in the world, *Bull. Int. Inst. Seismol. Earth Eng.*, 12, 39–58.
- Hirn, A., et al. (1984), Lhasa block and bordering sutures – a continuation of a 500-km Moho traverse through, *Nature*, 307, 25–27.
- Houseman, G., and P. England (1996), A lithospheric-thickening model for the Indo-Asian collision, In: *The Tectonic Evolution of Asia*, edited by A. Yin and T.M. Harrison, pp. 3–17, Cambridge Univ. Press, New York.
- Hudson, J. A. (2000), The effect of fluid pressure on wave speeds in a cracked solid, *Geophys. J. Int.*, 143, 302–310.
- Ismail-Zadeh, A. T., V. I. Keilis-Borok, and A. A. Soloviev (1999), Numerical modeling of earthquake flow in the south-eastern Carpathians (Vrancea): Effect of a sinking slab, *Phys. Earth Planet. Inter.*, 111, 267–274.
- Jade et al. (2004), GPS measurements from the Ladakh Himalayas, India: Preliminary tests of plate-like or continuous deformation in Tibet, *Geol. Soc. Amer. Bull.*, 116, 1385–1391.
- Keilis-Borok, V. I., I. M. Rotwain, and A. A. Soloviev (1997), Numerical modeling of block structure dynamics: dependence of a synthetic earthquake flow on the structure separateness and boundary movements. *J. Seismol.*, 1, 151–160.
- Le Pichon, X., M. Fournier, L. Jolivet (1992), Kinematics, topography, shortening, and extrusion in the India –Eurasia collision, *Tectonics*, 11(6), 1085–1098.
- Mazek, J. G., B. L. Isacks, and E. J. Fielding (1994), Rift flank uplift in Tibet: evidences for a viscous lower crust, *Tectonics*, 13, 659–667.
- Maksimov, V. I., and A. A. Soloviev (1999), Clustering of earthquakes in a block model of lithosphere dynamics, In: *Computational Seismology and Geodynamics 4*, D. K. Chowdhury (ed.), pp. 124-126, Amer. Geophys. Union, Washington, D.C.
- McClusky, S. et al. (2000), Global positioning system constraints on plate kinematics and dynamics in the eastern Mediterranean and Caucasus, *J. Geophys. Res.*, 105, 5695–5719.
- Meriaux, A.-S., F. J. Ryerson, P. Tapponnier, J. Van der Woerd, R. C. Finkel, X. Xu, Z. Xu, and M. W. Caffee (2004), Rapid slip along the central Altyn Tagh Fault: Morphochronologic evidence from Cherchen He and Sulamu Tagh, *J. Geophys. Res.*, 109, B06401, doi:10.1029/2003JB002558.
- Mogi, K. (1962), Magnitude-frequency relation for elastic shocks accompanying fractures of various materials and some related problems in earthquakes, *Bull. Earthquake Inst. Tokyo Univ.*, 40, 831–853.

- Molnar, P., and P. Tapponnier (1978), Active tectonics of Tibet, *J. Geophys. Res.*, **83**, 5361–5375.
- Narteau, C., P. Shebalin, M. Holschneider, J.-L. Le Mouél, and C. J. Allègre (2000). Direct simulations of the stress redistribution in the scaling organization of fracture tectonics (SOFT) model. *Geophys. J. Int.*, **141**, 1, 115–135.
- Nelson, K. D. et al. (1996), Partially molten middle crust beneath southern Tibet: synthesis of project INDEPTH results, *Science*, **274**, 1684–1688.
- Newman, W. I., D. L. Turcotte, and A. M. Gabrielov (1995), Log-periodic behavior of a hierarchical failure model with application to precursory seismic activation, *Phys. Rev. E*, **52**, 4827–4835.
- Panza, G. F., A. A. Soloviev, and I. A. Vorobieva (1997), Numerical modeling of block-structure dynamics: Application to the Vrancea region, *Pure Appl. Geophys.*, **149**, 313–336.
- Peltzer, G., and F. Saucier (1996), Present-day kinematics of Asia derived from geologic fault rates, *J. Geophys. Res.*, **101**, 27,943–27,956.
- Peltzer, G., and P. Tapponnier (1988), Formation and evolution of strikeslip faults, rifts, and basins during the India-Asia collision: An experimental approach, *J. Geophys. Res.*, **93(B12)**, 15,085–15,117.
- Peltzer, G., P. Tapponnier, and R. Armijo (1989), Magnitude of Late Quaternary left-lateral displacements along the north edge of Tibet, *Science*, **246**, 1285–1289.
- Royden, L. H., B. C. Burchfiel, R. W. King, Z. Chen, F. Shen, and Y. Liu (1997), Surface deformation and lower crustal flow in eastern Tibet, *Science*, **276**, 788–790.
- Searle, M. P., R. F. Weinberg, and W. J. Dunlap (1998), Transpressional tectonics along the Karakoram fault zone, northern Ladakh: constraints on Tibetan extrusion. In: *Continental Transpressional and Transtensional Tectonics*, Holdsworth, R. E., Strachan, R. A. and Dewey, J. F., Eds. Geological Society, London, Special Publication, **135**, 307–325.
- Shapiro, N. M., M. H. Ritzwoller, P. Molnar, and V. Levin (2004), Thinning and flow of Tibetan crust constrained by seismic anisotropy, *Science*, **305**, 233–236.
- Shaw, B. E., J. M. Carlson, and J. S. Langer (1992), Patterns of seismic activity preceding large earthquakes. *J. Geophys. Res.*, **97**, 479–492.
- Shebalin, P., I. Zaliapin, and V. Keilis-Borok (2000). Premonitory raise of the earthquakes' correlation range: Lesser Antilles. *Phys. Earth and Planet. Inter.*, **122**, 3–4, 241–249.
- Shen, Z. K., Zhao, C., Yin, A., Lin, Y., Jackson, D.D., Fang, P., and Dong, D. (2000), Contemporary crustal deformation in East Asia constrained by Global Positioning System measurements, *J. Geophys. Res.*, **105**, 5721–5734.
- Soloviev, A. A. (1995). Modeling of block structure dynamics and seismicity. In *European Seismological Commission, XXIV General Assembly, 1994 September 19–24, Athens, Greece, Proceedings and Activity Report 1992–1994*, Vol.III. University of Athens, Faculty of Sciences, Subfaculty of Geosciences, Department of Geophysics & Geothermy, pp. 1258–1267.
- Soloviev, A. A., I. A. Vorobieva, and G. F. Panza (1999), Modeling of block-structure dynamics: Parametric study for Vrancea, *Pure and Appl. Geophys.*, **156**, 395–420.
- Soloviev, A., and A. Ismail-Zadeh (2003), Models of dynamics of block-and-fault systems, In: *Nonlinear Dynamics of the Lithosphere and Earthquake Prediction*. V. I. Keilis-Borok and A. A. Soloviev (eds), pp. 71–139, Springer-Verlag, Berlin-Heidelberg.
- Stein, R. S. (1999), The role of stress transfer in earthquake occurrence, *Nature*, **402**, 605–609.
- Tapponnier, P., et al. (1981), Mesozoic ophiolites, sutures, and large-scale tectonic movements in Afghanistan, *Earth Planet. Sci. Lett.*, **52**, 355–371.

- Tapponnier, P., G. Peltzer, A. Y. Le Dain, R. Armijo, and P. Cobbold (1982), Propagating extrusion tectonics in Asia: New insights from simple experiments with plasticine, *Geology*, 10, 611–616.
- Tapponnier, P., X. Zhiqin, B. Meyer, F. Roger, N. Arnaud, G. Wittlinger, and Y. Jingsui (2001), Asymmetric, stepwise rise and growth of the Tibet Plateau, *Science*, 294, 1671–1677.
- Tod, S. R. (2002), The effects of stress and fluid pressure on the anisotropy of interconnected cracks, *Geophys. J. Int.*, 149, 149–156.
- Turcotte, D. L. (1997). *Fractals and Chaos in Geology and Geophysics*. 2nd Ed., Cambridge, University Press, 398 pp.
- Utsu, T., and A. Seki (1954), A relation between the area of aftershock region and the energy of main shock, *J. Seismol. Soc. Japan*, 7, 233–240.
- Vergne, J. et al. (2002), Seismic evidence for stepwise thickening of the crust across the NE Tibetan Plateau, *Earth Planet. Sci. Lett.*, 203, 25–33.
- Wang et al. (2001), Present-day crustal deformation in China constrained by Global Positioning System measurements, *Science*, 294, 574–577.
- Wittlinger et al. (1998), Tomographic evidence for localized lithospheric shear along the Altyn Tagh Fault, *Science*, 282, 74–76.
- Wittlinger, G., J. Vergne, P. Tapponnier, V. Farra, G. Poupinet, M. Jiang, H. Su, G. Herquel, and A. Paul (2004), Teleseismic imaging of subducting lithosphere and Moho offsets beneath western Tibet, *Earth Planet Sci. Lett.*, 221, 117–130.
- Wright, T. J., B. Parsons, P. C. England, and E. J. Fielding (2004), InSAR observations of low slip rates on the major faults of western Tibet, *Science*, 304, 236–239.